IMPROVEMENTS IN THE ACQUISITION OF DAYLIGHT ELECTROLUMINESCENCE IMAGES USING HIGH SPEED CAMERAS: COMPARISON OF SQUARE AND SINUSOIDAL WAVES EXCITATIONS

C. Terrados, D. González-Francés, J. Anaya, K.P. Sulca, V. Gómez-Alonso, M.A. González, O. Martínez*
GdS-Optronlab group, Dpto. Física de la Materia Condensada. Universidad de Valladolid
Edificio LUCIA. Paseo de Belén, 19. 47011 Valladolid (Spain)
*oscar.martinez@uva.es

ABSTRACT: Electroluminescence (EL) imaging is a very powerful technique for the identification of defects in Silicon solar cells and panels. Daylight Electroluminescence (dEL) has emerged recently, aiming to avoid the need to perform the EL images on dark environments, which complicates the measurements and limits the number of panels to be inspected. In this work we present a procedure to obtain dEL images by using sinusoidal or square excitations and high speed InGaAs cameras, working in asynchronous mode between excitation and signal capture. We subsequently apply post-processing techniques based on both frequency and time domain analyses to assess the quality of the images by quantifying the signal-to-noise ratio arising from both analyses. We captured a stack of dEL images using two InGaAs cameras capable of acquiring at speeds of up to 60 and 600 frames per second. Our results demonstrate the promising potential of the proposed dEL method, as the post-processed image stack exhibits the same features as dark EL images obtained using the same InGaAs cameras. Notably, this stack of dEL images can be obtained within a very short acquisition time, typically ranging from 100 to 200 ms, while maintaining good image quality.
Keywords: Electroluminescence, defect characterization, solar plants

1 INTRODUCTION

Electroluminescence (EL) characterization has become a widely accepted method for obtaining detailed information about the defects in Si solar cells and modules. This technique offers high spatial resolution, enabling precise detection of faults such as cracks, broken cells, interconnections, shunts, potential and light-induced degradation (PID/LID), among others [1, 2]. EL imaging is now a very well-established technique [2], providing complementary, and often more comprehensive, information compared to infrared thermography (IRT) and I-V characterization [3, 4]. However, two bottlenecks appear in performing the EL characterization, especially in the case of a large number of solar panels. First, EL is usually performed in dark scenarios. Secondly, EL requires the injection of current into the solar modules, which when performed on-site requires large power sources or frequent movement of a small power source from module to module.

Given the significant number of solar modules in a photovoltaic plant, the industry requires fast inspection techniques [5]. However, a massive inspection is currently unavoidable if the EL image is taken in strictly dark conditions, disassembling the modules and sending them to a lab, or also using specialized dark containers or mobile vans. Performing on-site EL during the night is also possible, but the risk of electrical manipulation damage is high and the potential number of modules to be inspected is low. For this reason, it would be very beneficial to perform on-site EL at the solar plant without disassembling the modules and during the day. This will reduce the risk of electrical manipulation damage, as well as to suppress the risk during assembly and disassembly of the modules, allowing a faster inspection of a large number of panels.

Daylight EL (dEL) has gained rapid development and significant attention in recent years [6-10], although it is still challenging to be applied in-situ in photovoltaic plants for a large number of modules. Enabling dEL requires IR based cameras – such as those based on InGaAs sensors–, in conjunction with sophisticated filtering procedures, capable distinguish the weak luminescence emission coming from the solar module from the more intense ambient light.

Several approaches for the obtention of dEL images can be used [10-12]. In our first approach [10], we used an InGaAs camera, a power source, and a mechanism for the injection of the current in a switching mode, with “on” and “off” periods. In this mode, there is a synchronization between the current injection and the acquisition of the images, in both “on” and “off” periods. The subtraction of the images obtained in both periods, and the accumulation of periods, give enough signal to obtain final good images, even at high irradiation conditions [10]. However, relatively long total acquisition times (of the order of tens of seconds) would be needed, especially for hard conditions, such as high irradiation conditions, low emitting panels, etc.

On the other hand, specific power sources able to produce square, sinusoidal, and other kinds of wave forms, can now being applied for the current injection of the solar modules. This can be used for the decoupling of the EL image acquisition and the power injection process (non-synchronized way). To do this, InGaAs cameras capable of capturing a large number of frames per second (fps) are needed, as well as robust post-processing analysis of the collected images.

Our proposed asynchronous dEL method enables the inspection of a large number of Si modules of a PV solar plant in very short times, which is becoming a requirement for O&M activities of a medium-to-large PV solar plant. We achieve this thanks to the combination of a 15 kW power source with square and sinusoidal wave forms, used for the injection of current into the strings, and a very fast acquisition of images. In this work we show the capability of two cameras from different manufacturers, with maximum acquisition speeds of 60 and 600 fps. Finally, the use of advanced filtering techniques to discard the non-EL related radiation is shown by comparing two methods to filtrate the EL signal from the ambient light: a time-domain method using square waves for the injection of current, and a frequency-domain method using both square or sinusoidal waves for the injection of current.

2 EXPERIMENTAL DESCRIPTION

For the current injection, a 15 kW power source was used (EA-PS 91500-30 3U 19" 3U 15000W model), allowing for the injection of current with I_{sc} values for a whole solar PV string. The power source allows for both square and sinusoidal wave form injection schemes for the excitation of Si solar modules.

Two InGaAs cameras, with maximum of 60 and 600 frames per second (fps), respectively, were used and compared in this work. A Hamamatsu C12741-03 InGaAs camara, with 640 x 512 pixels and pixel pitch of 20 x 20 µm, with 14 bits´ quantization and maximum speed of 60 fps, and a First Ligh C-RED 2 Lite InGaAs camera, with 640 x 512 pixels and pixel pitch of 15 x 15 µm, with 14-bit quantization and 16-bit dynamical range with maximum speed of 600 fps, were used. We use a Kowa short wave infrared (SWIR) optical system with 16 mm focal length for image acquisition. This allows an entire module per image to be viewed with the camera placed 2.5 meters away from the module. On the other hand, in order to suppress as much ambient light as possible, a SWIR bandpass filter, centered around 1160 nm with a bandwidth of 150 nm and a transmittance close to 90%, is used.

For the wave excitation, various frequencies (f) were tested while keeping the maximum intensity around I_{sc}. Additionally, exposure times (t_{exp}) were varied from 1.2 to 10 ms, depending on the selected acquisition velocity (number of fps) of the camera and irradiation conditions.

To conduct this analysis both a multi-Si Al-BSF (Sharp, ND-AR330H 330 W, V_{oc}=45.5 V, I_{sc}=9.40 A) and a multi-Si PERC module (Canadiansolar, CS6U 345 W, V_{oc}=46 V, I_{sc}=9.69 A) were used as test specimens.

3 DATA ANALYSIS

3.1 Square and sinusoidal wave excitation

Opposite to our previous synchronous method to obtain the dEL images of the modules [10], here we describe the use of an asynchronous scheme in which the excitation of the module and the acquisition of the images are decoupled. To do this, a periodic oscillating signal is needed, for which both square and sinusoidal schemes have been used for the current injection. The true EL signal coming from the module is discriminated from the ambient light (noise) by filtering the non-modulated component of the light acquired by the camera.

It is worth noting that the EL emission can be very small when compared with the background light, particularly for high irradiation conditions and older technology panels. This makes it challenging to distinguish signal from noise. Fig.1 illustrates this phenomenon for a multi-Si Al-BSF solar panel exposed to 750 W/m^2 of solar irradiation. The panel was excited with a sinusoidal wave of 10 A in amplitude, a frequency of 4 Hz with 10 ms of exposure time and recorded at 32 fps. In the image the average of the intensity recorded for each frame by the First Light camera vs the number of acquired frames is shown. Under these conditions the EL signal is only a very small fraction of the recorded intensity, with a modulated signal of less than 20 units over a background of ~11500 units. To make things worse, the background is not constant due to changes in the ambient light during the acquisition of the images which lead to a strong modulation of the background (see for instance Figure 1, the initial jump in the first 100 frames). It is worth noting that the longer the time required to record the stack of images the worse this modulated background can be, and more difficult is to extract the information from the panel. Consequently, a robust baseline correction step is imperative for each pixel in the image stack before differentiating modulated light from background light.

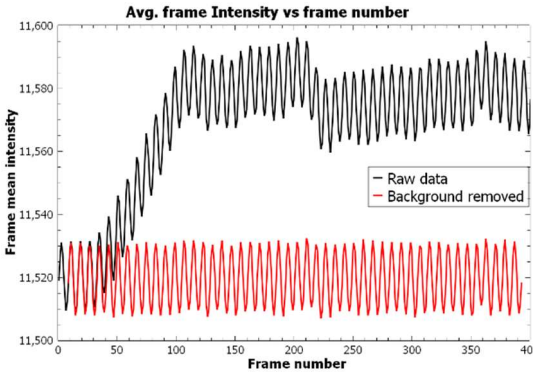

Figure 1: Intensity levels of the signal captured with the First Light camera (400 images) for the multi-Si Al-BSF module with a sinusoidal function. G = 750 W/m^2, f = 4 Hz, 32 *fps*, t_{exp} = 10 ms.

3.2 Frequency domains analysis

In the frequency domain, both sinusoidal and square waves can be processed by calculating the real valued Fast Fourier Transform (FFT) of each pixel in the image stack. In this process, we extract the signal to noise ratio (SNR) of the excitation frequency against the background defined in the region $[f/2, 2f]\backslash\{f\}$. The SNR is calculated from the squared amplitude at frequency f and the variance of the noise level in the specified region of the frequency spectrum signal analysis:

$$SNR = \begin{cases} 10log_{10}\left(\frac{(Peak\ amplitude)^2}{Var(Noise)}\right) & if > 10 \\ 0 & if \leq 10 \end{cases}$$

All pixels with SNR lower than 10 dB (i.e., equivalent to a signal three times higher than the standard deviation of the noise) are filtered, as they may not be distinguishable from noise with sufficient certainty as per the standard practice in signal analysis in frequency domain. As a quality metric the average SNR of the pixels in the lower quartile is defined (SNR_{25}=$Avg(Q1(\text{SNR}))$; i.e., the average SNR of those pixels with the lowest values which are associated with the regions with weakest EL emission. Therefore, the higher is this value, the better we can distinguish the weakest part of the image from noise. Finally, all frequencies but the excitation frequency f for sinusoidal waves, and odd multiples of f for square waves, [f, 3f, 5f, ...], are set to 0. Then the image stack is transformed to time domain to recover the image in real space containing only the EL component of the light. The last step is integrating the new image stack and normalizing to the number of periods to recover a single image with all the EL information. After this process, a final assessment quantifies the information recovered in the filtered image, typically represented as the number of bits needed to represent the bandwidth of the image. This measurement is based on the number of levels needed to represent the average of the most intense decile of pixels in the image to weight for potential spurious pixels (labelled here as Resolution).

3.3 Time domain analysis

In this process the *On* states are separated from the *Off* states, and therefore only square waves can be handled. After separating the *On* and *Off* states their averages are computed, and their difference is calculated for each pixel. The SNR is calculated using the same principles as described for frequency domain, but in this case the signal is the square of the average difference between the On and *Off* sates, and the noise is the variance of the *Off* levels. The variance is determined by averaging the variance of the *Off* states per period if there are more than 4 data points in an *Off* state during each period. Otherwise, the total variance of the *Off* states in the image stack is used. This is done to mitigate the effect of the residual background discussed in 3.1. For this analysis all pixels with less than 3 dB (i.e., equivalent to approximately 92% certainty of the pixel not being noise if noise is normally distributed) are filtered:

$$SNR = \begin{cases} 10\,log_{10}\left(\dfrac{\left(On_{avg} - Off_{avg}\right)^2}{Var(Noise)}\right) & if > 3 \\ 0 & if \leq 3 \end{cases}$$

The quality metric is identical to the one defined for frequency domain, the average SNR of the pixels in the lower quartile, $SNR_{25}=Avg(Q1(\text{SNR}))$. It is worth noting even being the same SNR_{25} for both types of analysis the numbers are not directly comparable because their detection threshold differs. This is because in time domain we are working with averages of the whole image stack, which are less sensitive to detect modulation in the signal than the frequency analysis which uses information of all individual frames in the image stack.

4 RESULTS DISCUSSION

4.1 Square and sinusoidal wave excitation

Figure 2 shows the dark EL image obtained with the Hamamatsu camera for the PERC module, which is the image against we benchmark the dEL images. In this case, the *Off* signal has been first collected, then the *On* signal for a constant current injection of 9 A (I_{sc}) has been collected. An artificial square image has been constructed using both *On* and *Off* signals, in order to create a synthetic image stack of 400 images like those obtained when exciting with a square signal with f=2.5 Hz, 50 fps, and t_{exp} = 15 ms.

A time domain analysis as described in 3.3 has been performed in this synthetic dataset, which result is the final dark EL imaged showed in Figure 2. The SNR_{25} marker in this case is ~63.6 dB, due to the completely dark conditions. The information recovered from this image stack has a resolution of ~11.2 bits, namely 2353 levels are needed to represent all the EL information from the image stack.

Figure 3(a, b) shows the processed dEL images for both sinusoidal and square excitations schemes on the same PERC module shown in Figure 2. Image stacks of 400 frames were acquired using the same camera, with f = 10 Hz, 46 fps and t_{exp} = 2 ms (G = 875 W/m^2). SNR_{25} values are in the order of 25 dB, indicating that even the weakest part of the image is filtered with a signal 8 times above the variance of the noise level, resulting in images where it is possible to clearly distinguish the state of all the cells of the module and their defective areas. Indeed, the visual information is almost indistinguishable from the image obtained in dark conditions. It is worth noting that the SNR_{25} is slightly better for the sinusoidal wave, while the square wave conveys slightly more information. Nonetheless, both types of excitations produce nearly indistinguishable results. When comparing the amount of information in these images, only approximately 8 out of the original 14 bits have been recovered. In other words, approximately 256 levels are recovered from the original 16384 levels of the camera sensor, which is nearly a tenfold reduction compared to the dark image. Therefore, both types of panel excitation, square and sinusoidal, when properly generated, will result in similar image quality and there is no clear reason to prefer one over the other. However, by exciting with square waves we allow for a time processing of the image, which is not currently achievable with the sinusoidal wave.

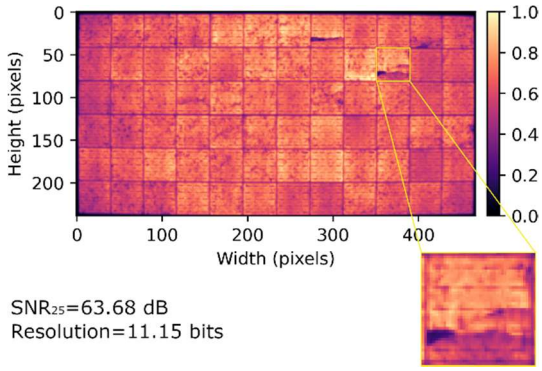

Figure 2: Dark EL image of the PERC module obtained with the Hamamatsu camera working with an acquisition velocity of 50 fps and t_{exp} = 15 ms. In order to compare the quality of the image with the dEL images shown in figure 3, a virtual square wave has been generated, with f = 2.5 Hz, and a post-process analysis has been carried out in the time domain. The inset shows the zoom for a single cell with dark areas and a crack.

Figure 3(c) shows the processed image of the PERC module with square excitation and time domain analysis. Once again, the image quality is sufficient to clearly distinguish the same features as in dark conditions and nearly indistinguishable from the frequency domain analysis. It's worth noting that the difference in the SNR_{25} metric between time and frequency analysis is attributed to the distinct mathematical procedures used in the analysis as described in 3.2 and 3.3. In any case, we can perform a direct comparison with the image shown in Figure 2 since both are processed with the same method. By doing this, it is observed that, although the dEL image is visually comparable with the dark EL image, the quality markers are very different. In dEL we are recovering only ~222 levels to represent the image, i.e. we have 10 times less resolution than in dark EL. However, even with this loose in recovered information both dark EL and dEL allow to recognise the same defective regions and even small features in the panel. This confirms the capability of the dEL process in the non-synchronized way carried out in this work.

4.2 Comparison between cameras with different acquisition velocities

Very recently, a new generation of InGaAs cameras with very high acquisition velocities have appeared in the market. This paves the way for a much faster acquisition

of the dEL images. In order to test the capabilities of such cameras, we have tested the First Light C-RED 2 Lite InGaAs camera, with a maximum acquisition velocity 10 times higher than the one used in Figures 2 and 3 (600 fps vs 60 fps). This increase in the acquisition velocity means also a decrease of the maximum exposure time, and therefore potentially to a more challenging filtering of the background light if the sensors are not able to detect more efficiently the photons from the panel.

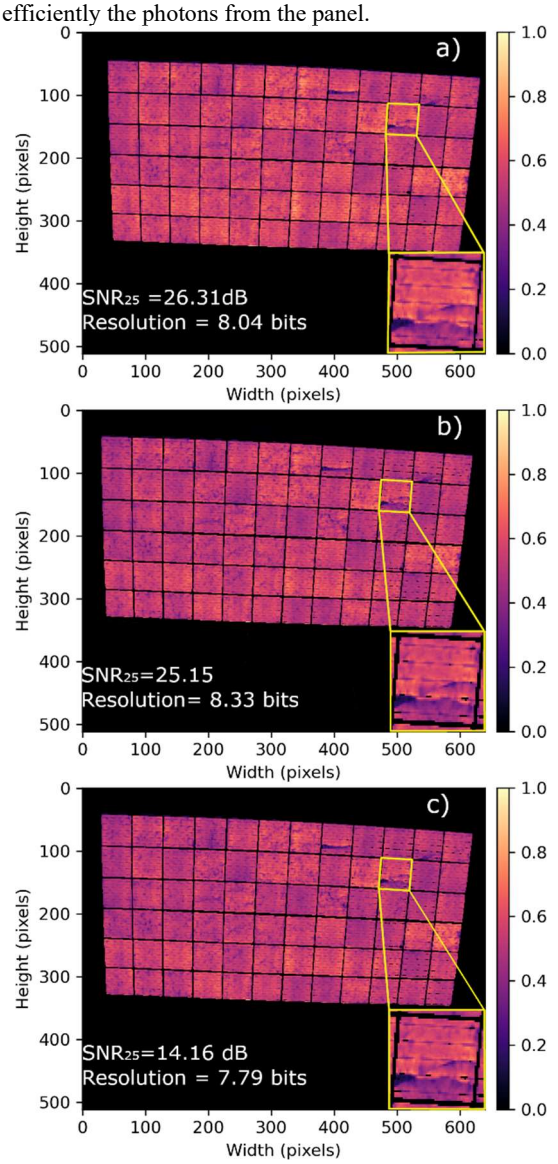

Figure 3: dEL images of the PERC module obtained with the Hamamatsu camera and with sinusoidal (a) and square (b, c) wave excitations. The post-process analysis has been done in the frequency domain (a, b) or in the time domain (c). G = 875 W/m^2, f = 10 Hz, 46 fps, t_{exp} = 2 ms. The inset in each image shows the zoom for a single cell with dark areas and a crack.

Figure 4 (a, b) shows the dEL images obtained with both the Hamamatsu and the First Light cameras, respectively. A square wave excitation was used in both cases. The acquisition conditions were f = 2 Hz, 46 fps, t_{exp} = 2 ms to obtain 400 images with the Hamamatsu camera, and f = 62.5 Hz, 600 fps, t_{exp} = 1.2 ms to obtain 594 images with the First Light camera. It should be noted that the measurements with both cameras were taken in different days, and unfortunately the irradiance conditions were different, G = 780 W/m^2 and 340 W/m^2 for the Hamamatsu and First Light, respectively. To somewhat compensate for this low irradiance, we have selected for this comparison a more challenging panel which has a much weaker EL response than the previously described PERC panel. Therefore, an older multi-Si Al-BSF module was selected for this comparison. A post-process analysis in the frequency domain was performed in both cases, yielding SNR_{25} and Resolution values of 20.36 dB and 9.06 bits for the Hamamatsu camera and 18.02 and 9.53 bits for the First Light camera. In both cases the images yield similar level of information and allow to clearly detect all the features shown by the dark EL image from that module, Fig. 4 c, which was obtained with the Hamamatsu camera for comparison. It should be noted that the images were obtained at different temporal moments, and the module has degraded in the last images (obtained with the Hamamatsu camera) respect to the image obtained with the First Light camera.

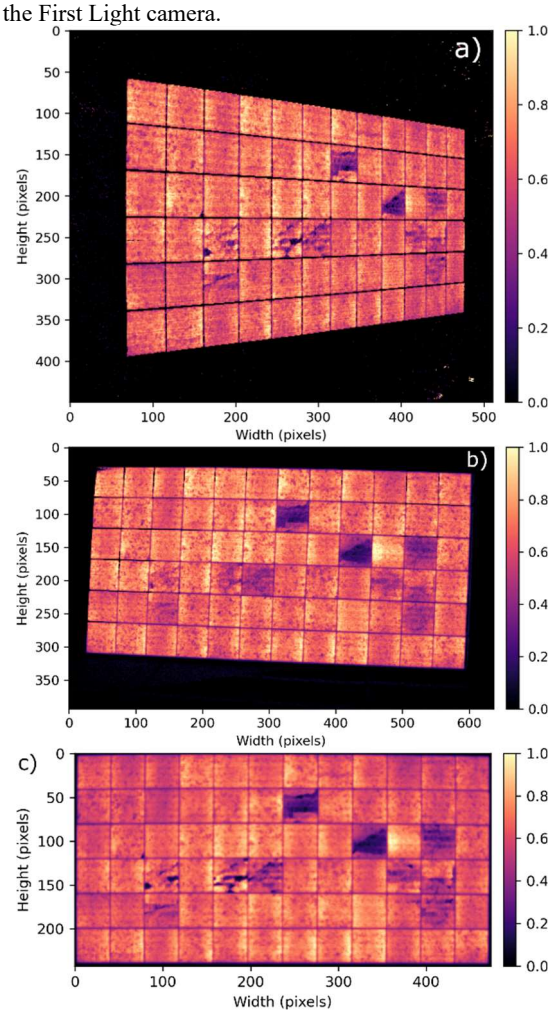

Figure 4: dEL images of the multi-Si Al-BSF module obtained with both the Hamamatsu camera (a) and the First Light camera (b) with square wave excitations. The post-process analysis has been done in the frequency domain. In a) G = 780 W/m^2, f = 2 Hz, 46 fps, t_{exp} = 2 ms. In b) G = 340 W/m^2, f = 62.5 Hz, 600 fps, t_{exp} = 1.2 ms. (c) Dark EL image of the same module obtained with the Hamamatsu camera working with an acquisition velocity of 32 fps and t_{exp} = 15 ms. An artificial square wave has been generated, with f = 2 Hz, and a post-process analysis has been done in the frequency domain.

Figure 4 shows that working with short exposure times and fast acquisition times is not linked to a worsening of the dEL image quality, and therefore it opens the door to perform the analysis in much shorter times. Note that the Hamamatsu camera needed ~8.7 s to collect all the images while the First Light used slightly less than 1 s even collecting 50% more images.

To test how much we can reduce the time needed to obtain a final image with enough quality we have removed frames from the 594 image stack taken with the First Light camera. For this we have removed full periods of data from the end of the stack and extracted the SNR_{25} marker from the resultant image stack. This analysis is shown in Fig. 5 for both frequency and time domains. Here it is observed that for frequency domain analysis by increasing the number of periods from 5 up to 20 the SNR_{25} value increases, then reaching a plateau until 40 periods, and then degrades for 50 and 60 cycles. This behaviour occurs because the signal degrades in frequency over time, likely due to fluctuations in the background light that introduce a small phase shift when subtracting the baseline. This figure demonstrates that there is little improvement in image quality when extending the measurement time from ~100 ms to ~600 ms, and in some cases, extending the measurement time beyond that limit can result in worse dEL images. On the other hand, for the time domain analysis the SNR_{25} slightly increases monotonically with the number of cycles/frames in the stack (Figure 5-a, left axis). This improvement occurs because the difference between the average and noise level becomes more significant as more data is added, while it is less sensitive to phase degradation. When evaluating the resolution of the final images, a pattern akin to that observed for the SNR_{25} marker in frequency analysis becomes evident. Specifically, the resolution plateaus at 10 periods and exhibits a slight degradation when exceeding 40 periods. In contrast, in the time-dependent analysis, resolution displays a nearly constant trend regardless of the number of periods. As previously discussed, this behaviour is expected since the addition of more periods primarily enhances the ability to discriminate signal from noise rather than amplifying the signal level itself.

This finding illustrates that remarkably short acquisition times (~160 ms) are sufficient for acquiring dEL images in very short timeframes, paving the way to the implementation of dEL in the field using cameras installed on drones for efficient inspection of a large number of modules.

5 CONCLUSIONS

Large improvements for the obtention of dEL images have been proven, with the combined use of a 15 kW power source with square and sinusoidal waves excitation modes and a very high acquisition speed camera. Two methods for analyse the dEL signal from Si solar panels have been disclosed: one in the frequency domain and one in the time domain. Both methods have been applied to images taken from multi-Si low emitting (Al-BSF) and high emitting (PERC) panels. It is demonstrated that, with proper data filtering, the information recovered from dEL images can show a similar amount of visual information than images taken in dark conditions. A metric (SNR_{25}) has been proposed to quantify the quality of the images. dEL images with good quality can be obtained in very short timeframes (approximately 160 ms). These improvements in the acquisition of the images can open the door for the massive inspection of Si solar plants by a very powerful technique such as EL imaging.

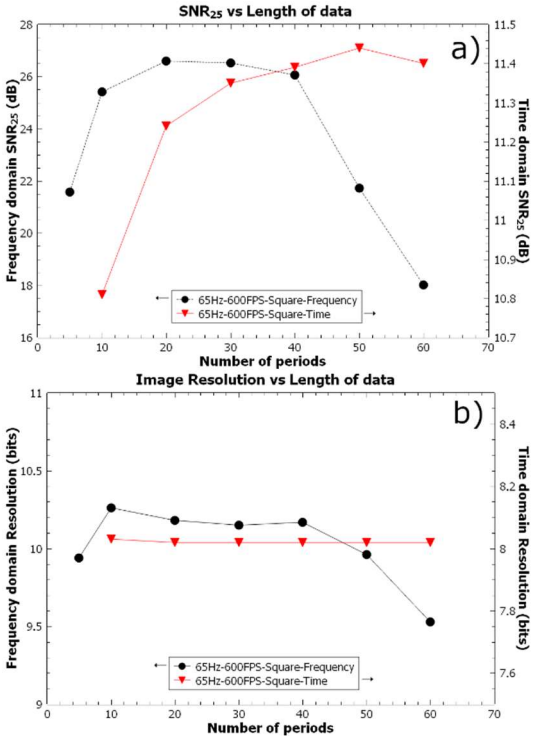

Figure 5: SNR_{25} evolution as a function of the number of analysed cycles (a). The data correspond to the dEL images of the multi-Si Al-BSF module obtained with the First Light camera with square wave excitation. The post-process analysis has been done both in the frequency and time domains. G = 340 W/m^2, f = 62.5 Hz, 600 fps, t_{exp} = 1.2 ms. Also, the evolution of the resolution of the images with the number of periods is shown (b).

6 ACKNOWLEDGMENTS

This work has been financed by the Spanish Ministry of Science and Innovation, under project PID2020-113533RB-C33, and by the Regional Government of Castilla y León (Junta de Castilla y León) and by the Ministry of Science and Innovation and the European Union NextGenerationEU / PRTR under the project "*Programa Complementario de Materiales Avanzados*".

7 REFERENCES

[1] L. Koester, S. Lindig, A. Louwen, A. Astigarraga, G. Manzolini, and D. Moser, "Review of photovoltaic module degradation, field inspection techniques and techno-economic assessment," Renew. Sustain. Energy Rev., vol. 165, no. November 2021, p. 112616, 2022, doi: 10.1016/j.rser.2022.112616.

[2] IEC, "IEC TS 60904-13 Photovoltaic Devices - Part 13: Electroluminescence of Photovoltaic Modules," http://www.iec.ch/. [Online]. Available: http://www.iec.ch/

[3] S. Gallardo-Saavedra, L. Hernández-Callejo, M.C. Alonso-García, J.D. Santos, J.I. Morales-Aragones, V.

Alonso-Gómez, A.M. Moretón-Fernández, M.A. González-Rebollo, O. Martínez, "Nondestructive characterization of solar PV cells defects by means of electroluminescence, infrared thermography, I-V curves and visual tests: Experimental study and comparison". Energy 205, 117930 (2020).

[4] M. Aghaei, A. Fairbrother, A. Gok, S. Ahmad, S. Kazim, K. Lobato, G. Oreski, A. Reinders, J. Schmitz, M. Theelen, P. Yilmaz, J. Kettle, "Review of degradation and failure phenomena in photovoltaic modules". Renew. Sustain. Energy Rev. 159, 112160 (2022).

[5] I. Høiaas, K. Grujic, A. Gerd, I. Burud, E. Olsen, N. Belbachir, "Inspection and condition monitoring of large-scale photovoltaic power plants: A review of imaging technologies". Renew. Sustain. Energy Rev. 161, 112353 (2022).

[6] L. Stoicescu, M. Reuter, J.H. Werner, "Daysy: luminescence imaging of PV modules in daylight", in 29th Eur. Photovolt. Sol. Energy Conf. Exhib. (2014), p. 2553.

[7] J. Adams et al., “Non-Stationary Outdoor EL-Measurements with a Fast and Highly Sensitive InGaAs Camera,” 32nd Eur. Photovolt. Sol. Energy Conf. Exhib., 2016.

[8] T. J. Silverman, M. G. Deceglie, K. Vansant, S. Johnston, and I. Repins, “Illuminated Outdoor Luminescence Imaging of Photovoltaic Modules,” IEEE Photovolt. Spec. Conf., 2017.

[9] G. Alves Dos Reis Benatto et al., “Drone-Based Daylight Electroluminescence Imaging of PV Modules,” IEEE J. Photovoltaics, vol. 10, no. 3, pp. 872–877, 2020, doi: 10.1109/JPHOTOV.2020.2978068.

[10] M. Guada et al., “Daylight luminescence system for silicon solar panels based on a bias switching method,” Energy Sci. Eng., no. June, pp. 1–15, 2020, doi: 10.1002/ese3.781.

[11] C. Mantel et al., “SNR Study of Outdoor Electroluminescence Images under High Sun Irradiation,” in 2018 IEEE 7th World Conference on Photovoltaic Energy Conversion (WCPEC) (A Joint Conference of 45th IEEE PVSC, 28th PVSEC & 34th EU PVSEC), Jun. 2018, no. 1, pp. 3285–3289. doi: 10.1109/PVSC.2018.8548264.

[12] G. A. dos Reis Benatto et al., “Daylight Electroluminescence of PV Modules in Field Installations: When Electrical Signal Modulation is Required?,” in 8th World Conference on Photovoltaic Energy Conversion, 2022, pp. 735–739. doi: 10.4229/WCPEC-82022-3BV.3.44.